Article

Study on Single-Phase BLDC Motor Design through Drive IC Integration Analysis

Ye-Seo Lee [1], Na-Rim Jo [1], Hyun-Jo Pyo [2], Dong-Hoon Jung [3] and Won-Ho Kim [2,*]

[1]   Department of Next Generation Energy System Convergence, Gachon University,
     Seongnam 13120, Republic of Korea; aaabbb0127@gachon.ac.kr (Y.-S.L.); rimna22@gachon.ac.kr (N.-R.J.)
[2]   Department of Electrical Engineering, Gachon University, Seongnam 13120, Republic of Korea;
     vdsl00700@gachon.ac.kr
[3]   Department of Mechanical, Automotive and Robot Engineering, Halla University,
     Wonju 26404, Republic of Korea; dh.jung@halla.ac.kr
*   Correspondence: wh15@gachon.ac.kr

Abstract: In this paper, a single-phase BLDC motor is applied to a cooling fan motor and a Drive IC integration analysis method of the single-phase BLDC motor is proposed. Single-phase BLDC motors have a simple structure, are easy to manufacture, and are low cost, so they are used in applications where low outputs and low costs are advantageous. Single-phase BLDC motors use a full-bridge inverter (Drive IC), and this inverter (Drive IC) has dead time due to switching. Therefore, in order to consider dead time when analyzing a single-phase BLDC motor, analysis through integration with Drive IC is necessary. This paper compares the types of single-phase BLDC motors, designs a model that satisfies target performance, and conducts research on Drive IC integration analysis through FEA. A prototype motor was manufactured and tested, and the validity of the Drive IC integration analysis was verified.

1. Introduction

The existing microwave oven (MWO) cooling fan motor uses a 5W-rated shaded-pole induction motor (SPIM), as shown in Figure 1. The SPIM is characterized by a structure where the main concentrated winding is wound around the stator core, resulting in high losses in both copper and core, leading to low efficiency. However, due to its low cost, it is mainly used in low-power applications [1]. Although this type of induction motor has low efficiency and is unable to control variable speeds, it has the advantage of being simple to manufacture and having a stable structure. Accordingly, research has been conducted on design optimization for high performance and stable structure, as well as on cooling methods for high-loss induction motors [2] and on the accurate prediction of the stator winding temperature [3]. In the household appliance market, cost reduction has been prioritized over efficiency concerns, leading to the adoption of induction motors with low efficiency but competitive pricing. However, previously used SPIMs lacked speed control capabilities, requiring the use of different motors for fan applications that require different torque levels at different speeds. This resulted in an increase in fan motor management and operating costs. In this regard, research is needed to apply permanent magnet motors with high torque density, efficiency, and variable speed control to cooling fan motors. By replacing the existing SPIM with a permanent magnet motor, the use of variable speed control allows for the utilization of a single motor, thereby reducing management and operating costs. In addition, the higher output density in comparison to induction motors leads to a reduction in the use of magnets, windings, and cores.
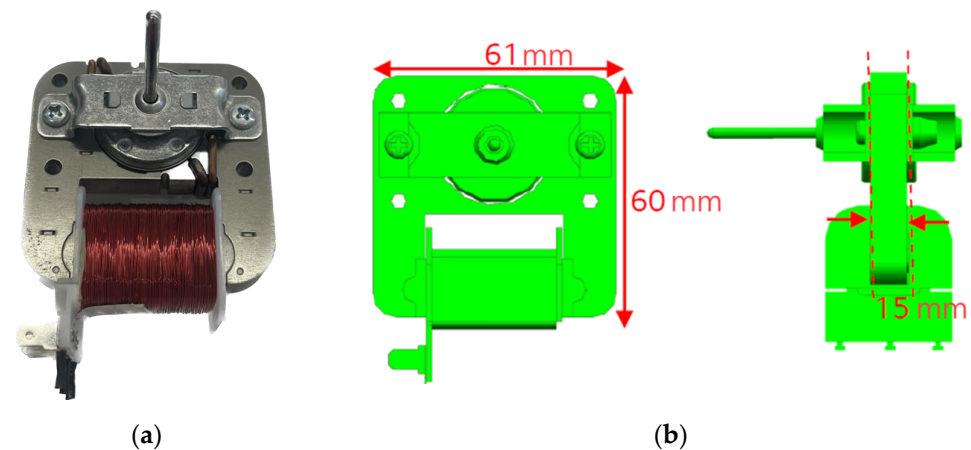
Figure 1. Existing cooling fan motor (SPIM): (**a**) cooling fan motor (SPIM); and (**b**) cooling fan motor (SPIM) size.

Permanent magnet synchronous motors are classified into radial flux motors (RFM) and axial flux motors (AFM), depending on the direction of the magnetic flux. AFM is a motor that is advantageous for applications where a short axial length is crucial, especially in fields where high output density is important. However, unlike the RFM, which has a small difference in torque density depending on the number of poles in the same volume, AFM has the characteristic of increasing torque density as the number of poles increases, so RFM is advantageous with its small number of poles [4]. RFMs are largely divided based on the magnet's position into interior permanent magnet motors (IPM) and surface permanent magnet motors (SPM). An IPM has magnets positioned inside the rotor core, resulting in a higher magnetic flux density compared to SPM [5]. However, IPMs present challenges in aligning the centers of the rotor and stator due to the magnet's location inside the rotor core, and this eccentricity leads to difficulties in manufacturing and generates magnetic saturation [6,7]. On the other hand, SPM has magnets positioned outside the rotor core toward the stator, and has a simple structure, which makes it easier to manufacture, more convenient to maintain, and more cost-effective to produce [8]. In this regard, research has been conducted to reduce the costs of permanent magnet motors, especially surface permanent magnet motors (SPM), which are easier to manufacture and have lower production costs. Studies have focused on reducing the cost of magnets as a means of general costs reduction. Research has been conducted on hybrid magnets aimed at reducing the cost of magnets, resulting in a 37.9% reduction in torque cost [8]. In addition, studies have been conducted to explore magnetic shapes that allow for a reduction in magnet usage and save processing time, thereby reducing both raw material and processing costs [9].

Permanent magnet motors are mainly used in three phase or single phase. Three-phase motors are driven by a rotating magnetic field and have a high power density, high power factor, and high output density. On the other hand, single-phase motors are driven by an alternating magnetic field and have a lower output density and higher torque ripple than three-phase motors. However, they have a simple structure and are cost-effective. Furthermore, single-phase motors have the advantage of low controller costs and simple manufacturing requirements, making them suitable for mass production [10–14]. As a result, three-phase motors are preferred in applications that require high output, while single-phase motors are preferred in household applications where low output and cost-effectiveness are advantageous. This paper focuses on the research of a single-phase surface permanent magnet BLDC motor, which has a simple manufacturing process, is cost effective and suitable for low output applications.

In this paper, a single-phase BLDC motor is applied to a MWO cooling fan motor, that requires a low output and low cost characteristics in a limited volume. To meet the performance requirements in a limited volume, this paper compares four types of single-

phase BLDC motors: R-Type, C-Type, internal rotor type, and external rotor type. The performance characteristics and cost comparisons between C-Type and external rotor types are analyzed, and a proposed external rotor type that satisfies cost savings is presented. In the design of a single-phase BLDC motor, an asymmetrical air gap structure was applied to ensure the starting torque by creating a phase difference in the cogging torque according to the characteristics of the single-phase motor driven by alternating magnetic fields. In addition, to account for the impact of dead time in the full-bridge inverter (Drive IC), a design using a Drive IC was assessed to ensure the accuracy of the analysis.

This paper consists of a total of five sections. In Section 2, the design considerations of a single-phase BLDC motor are discussed, including the torque equation, Drive IC integration analysis, and the structure required for starting torque. Section 3 compares four types of single-phase BLDC motors and designs a motor to meet the target performance for C-Type and external rotor single-phase BLDC motors that are advantageous in satisfying the target torque. Additionally, a performance comparison is conducted through analysis of integrated Drive IC. Section 4 selects the motor that meets the desired performance and cost-saving standards, and validates the Drive IC integration analysis through the production of a prototype motor. Section 5 summarizes the conclusions of this paper. The design and integration of the Drive IC in this paper were performed using Ansys 2022 Maxwell software and the validity of the proposed Drive IC integration analysis is verified through finite element analysis (FEA) and the production and testing of a prototype motor.

2. Considerations in the Design of a Single-Phase BLDC Motor

2.1. Torque Equation for a Single-Phase BLDC Motor

A single-phase BLDC motor is a maintenance-free motor due to the use of an electrical commutating mechanism instead of a commutator and brushes. It is widely used in applications that require compactness due to its less complex design in comparison to three-phase motors. In a BLDC motor, the torque varies because the magnetic resistance of the air gap varies depending on the rotor's position due to the stator teeth. Equation (1) represents the torque constant as a function of rotor position, Equation (2) represents the voltage equation for a single-phase BLDC motor, and Equation (3) represents the torque equation [15].

$$k_e = n \times \frac{\Delta \lambda}{\Delta \theta} \tag{1}$$

where λ is flux linkage of a coil, θ is the rotor position in radian, n is the number of coils in the series.

$$e_b = k_e(\theta,\, i) \times \omega$$
$$v_{io} = i \times R + L \times \frac{di}{dt} + e_b \tag{2}$$

$$T_m = k_e(\theta,\, i) \times i + T_{cg}(\theta) \tag{3}$$

where e_b is back EMF, k_e is EMF constant which is the function of the rotor position, i is winding current, ω is angular velocity, v_{io} is inverter output voltage, T_m is motor torque, and T_{cg} is cogging torque as a function of rotor position θ.

2.2. Single-Phase Drive IC Integration Analysis

For motor control, a single-phase BLDC motor can use either a single-phase half-bridge inverter or a single-phase full-bridge inverter. The half-bridge inverter circuit generates AC voltage for single-phase motors. The operation of the half-bridge inverter involves alternating the switches on and off at every half-cycle of the required AC voltage frequency period T. Equation (4) represents the fundamental and harmonic components of the inverter, and Equation (5) provides the root mean square (RMS) value of the fundamental voltage.

Based on Equation (5), the inverter can deliver 45% of the DC input voltage to the load in terms of the RMS value of the AC voltage.

$$v_p = \frac{2V_{dc}}{\pi} \sum_{n=1,3,5\cdots}^{\infty} \frac{sinn\omega t}{n} \ (n = 1,\ 3,\ 5,\cdots) \tag{4}$$

$$V_{p1-rms} = \frac{1}{\sqrt{2}}\frac{2V_{dc}}{\pi} = 0.45V_{dc} \tag{5}$$

Due to its inefficient utilization of DC voltage, the single-phase half-bridge inverter is not a suitable option for generating effective single-phase AC voltage. Therefore, the full-bridge inverter is used. Figure 2 represents the circuit and output voltage of the single-phase full-bridge inverter. In order to obtain an effective single-phase AC voltage, each voltage must be switched with a phase difference of 180 degrees. Therefore, switches D1, D2, and switches D3, D4 alternate between on and off states. The fundamental and harmonic components during that period are represented by Equation (6). The single-phase full-bridge inverter is predominantly used because it can obtain twice the AC voltage compared to the half-bridge inverter, all under the same DC voltage. The output voltage of the single-phase full-bridge inverter is provided in Equation (7), where the *H* Pole and *L* Pole represent the sections of switches as shown in Figure 2, with the H Pole corresponding to switches D_1 and D_4, and the L Pole corresponding to switches D_2 and D_3. V_H denotes the pole voltage for H Pole, V_L represents the pole voltage for L Pole, S_H is the switching function for H Pole, and S_L is the switching function for L Pole [16].

$$v_o = \frac{4V_{dc}}{\pi} \sum_{n=1,3,5\cdots}^{\infty} \frac{sinn\omega t}{n} \ (n = 1,\ 3,\ 5,\cdots) \tag{6}$$

$$\begin{aligned} v_H &= V_{dc}\left(S_H - \tfrac{1}{2}\right) \\ v_L &= V_{dc}\left(S_L - \tfrac{1}{2}\right) \\ v_o &= v_H - v_L = V_{dc}(S_H - S_L) \end{aligned} \tag{7}$$
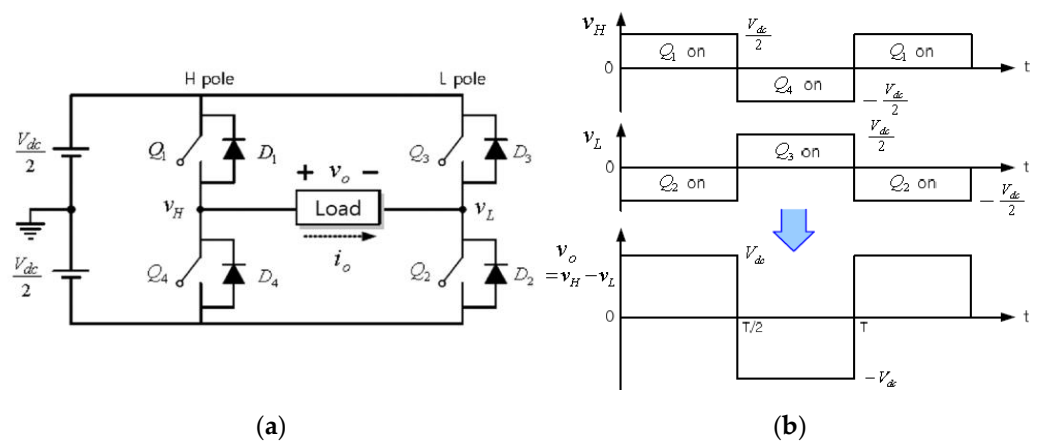

(a)   **(b)**

Figure 2. Single phase full-bridge inverter: (**a**) circuit; and (**b**) output voltage.

A single-phase inverter experiences shoot-through time during the intervals when switching occurs. In this case, there is a momentary period when all switches are simultaneously conducting, which can lead to a short circuit incident. To prevent such accidents during switching transitions, the switching time of the switches is intentionally delayed by a certain amount of time, referred to as 'dead time'. During the dead time, an error occurs

in the output voltage, and the average error voltage is provided in Equation (8). Where, t_{dead} represents the dead time, and f_{sw} represents the switching frequency [16].

$$V_{err} = t_{dead} V_{dc} f_{sw} \tag{8}$$

Furthermore, this dead time decreases the fundamental component of the output voltage and generates harmonics in the output voltage. A study has been conducted to reduce dead time [17].

The conventional design and analysis methods for single-phase BLDC motors did not take into account the inverter's dead time and assumed the inverter's output voltage to be ideal. When analyzing without considering the inverter's dead time, it is impossible to accurately account for the decrease in the output voltage's fundamental components and the generation of harmonic components due to dead time. Therefore, when analyzing single-phase BLDC motors, it is necessary to integrate a single-phase full-bridge inverter.

Figure 3 represents the circuit of the integrated single-phase full-bridge inverter. To integrate the single-phase full-bridge inverter, four elements are required: the inverter input voltage (V_{dc}), diode specifications, switch resistance (R_{on}), and two signals for the switches On and Off. The input voltage and diode specifications can be obtained from the inverter's specifications. Switch resistance can also be determined through the inverter's specifications, and it may vary depending on the circuitry of each Drive IC. Typically, the resistance or the switch is represented as the sum of the resistances for the two switches (S_1 and S_4 in Figure 3). When designing the motor, it is essential to match the inverter's current limit. The current value is influenced by the voltage drop component resulting from the switches. Thus, it is necessary to take into account the switch resistance. Finally, two signals are required for controlling the switching of the switches on and off. Figure 4 represents the waveform of the node voltage. Signal1 is connected to switches S_1 and S_4, while Signal2 is connected to switches S_2 and S_3. When the node voltage of the signals is greater than 0 V, the switches are ON, and when it is less than 0 V, the switches are OFF. To prevent the inverter from shoot-through, the ON and OFF times of each switch need to be delayed, and therefore, T_r and T_f in Figure 4 must be greater than 0.
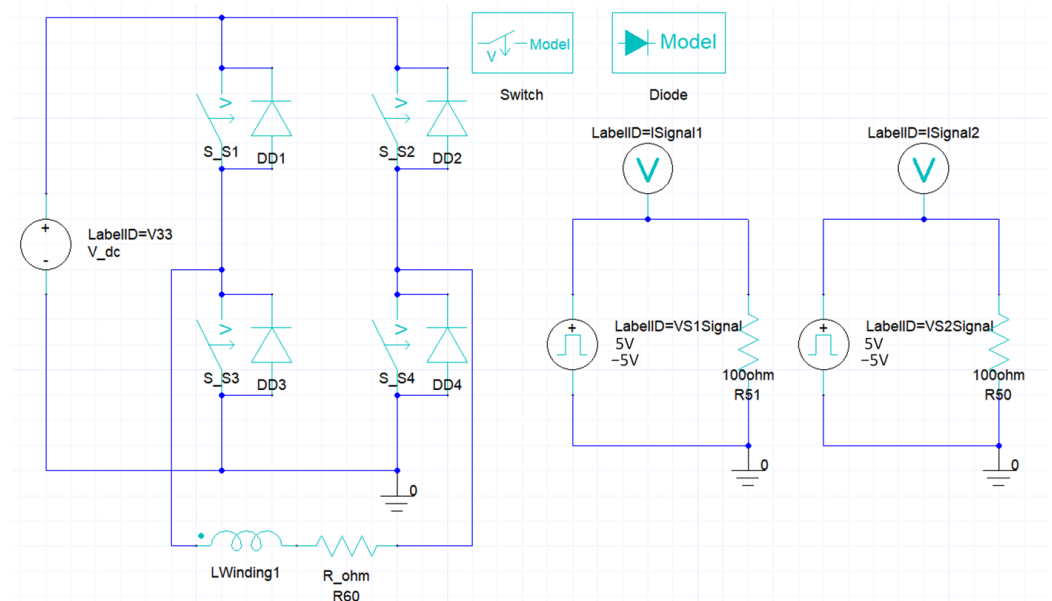

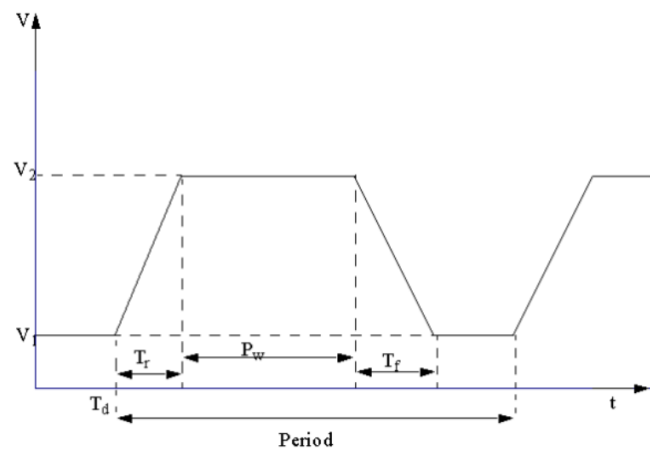**Figure 3.** Single-phase full-bridge inverter circuit diagram.

Figure 4. The T_r and T_f in the node voltage waveform.

The Drive IC's output voltage and current undergo rising segments during the dead time, which happens when the switches are toggled on and off. The soft ON and soft OFF function are used to prevent such rising phenomena. In the case of a Drive IC with the soft ON and soft OFF function, the angle of the registers can be adjusted to generate a smooth waveform for output. Figure 5 illustrates the voltage and current waveforms with and without implementation of the soft ON and soft OFF function. Where V_{OUT1} and V_{OUT2} represent the voltages when switches S_1 and S_4 are on and when switches S_2 and S_3 are on, respectively, in Figure 3. The rising portion of the output voltage is generated due to dead time, which affects the overall output. Therefore, when using a Drive IC with soft ON and OFF functionality, additional analysis is required. When using the soft ON and OFF function, the current waveform is smoothly regulated through the adjustment of the register angle. Therefore, in order to conduct an analysis, it is imperative to anticipate the scope of control. In this case, the lower magnitude of the current within the predicted range is chosen (1.63 A in Figure 6). This can be observed from the current waveform in Figure 6. Additionally, when considering the soft ON and soft OFF function, it is important to take into account the current limit of the Drive IC, which is based on the predicted current range (1.63 A to 1.71 A; shown in Figure 6).
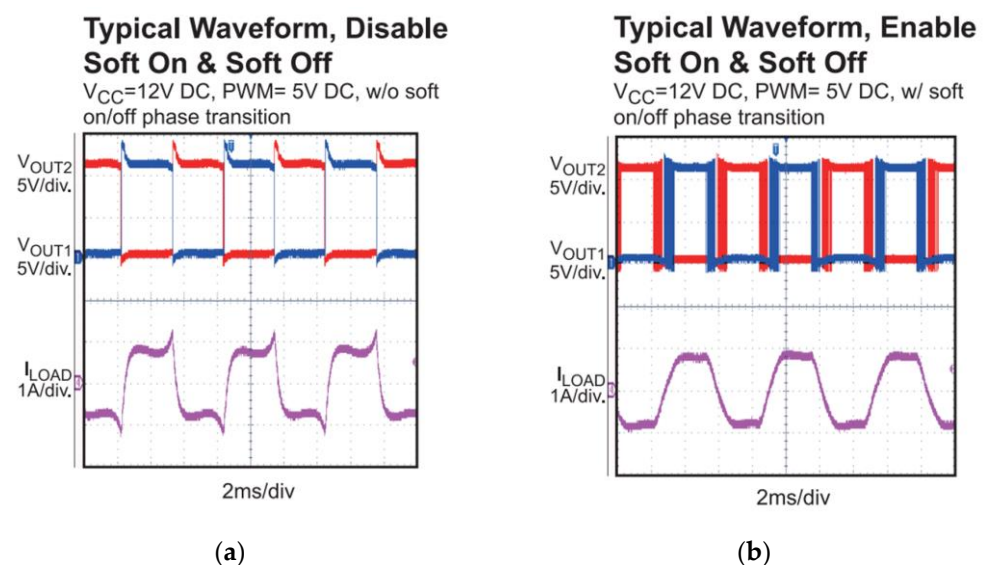

Figure 5. Soft ON and soft OFF control function: (**a**) Without using soft ON and soft OFF function; and (**b**) With soft ON and soft OFF function (MPS-MP6517B datasheet).
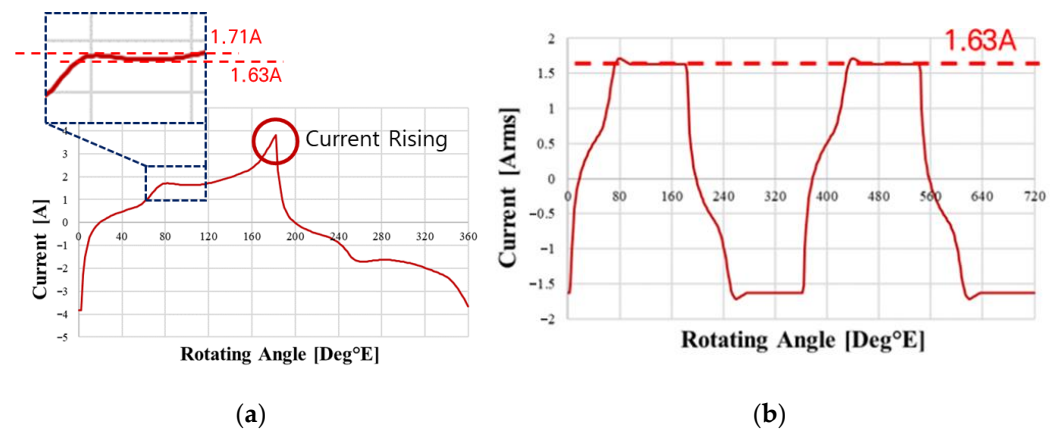
Figure 6. Current waveform with soft ON and soft OFF control: (**a**) Current waveform without using soft ON and soft OFF function; and (**b**) Expected current waveform when using the soft ON and soft OFF function.

In this paper, the final selection of the Drive IC with Switch ON and OFF functionality was made considering the voltage drop due to switch resistance and motor current limitations. When selecting a Drive IC, the maximum value of the switch resistance and current limit should be considered according to the performance and specifications of the motor.

2.3. The Asymmetric Air Gap Structure of a Single-Phase BLDC Motor

A single-phase brushless DC motor operates through the use of a mechanically generated alternating magnetic field, which occurs via the winding of coils on the stator. This differs from a three-phase brushless DC motor, which utilizes a rotor in its operation. Therefore, the stator typically has an equal number of poles and slots in a 1:1 ratio. When a single-phase brushless DC motor is in operation, the interaction between the rotor magnets and the stator teeth produces cogging torque. Additionally, the interaction between the stator current and the rotor magnets results in magnetic torque. A single-phase brushless DC motor with an equivalent number of poles and slots may produce magnetic torque that matches cogging torque. Additionally, at the point where the cogging torque becomes zero, the magnetic torque can exhibit negative torque. This creates a zero-torque region referred to as the "dead point". Due to the dead point, a single-phase BLDC motor becomes unable to start its operation [14]. Therefore, for single-phase motors utilizing the alternating field mechanism, it is essential to verify the availability of starting torque. To eliminate the dead point, it is common to apply an asymmetric air-gap shape. When an asymmetric air-gap shape is applied, a phase difference occurs in the cogging torque, preventing the occurrence of zero-torque regions. Research has been conducted to propose various shapes for asymmetric air-gap and analyze their performance characteristics [18–20].

To ensure the starting torque of the single-phase BLDC motor, this design utilized an asymmetric air gap shape. Figure 7 illustrates the shapes of the symmetric air-gap model and the model with an applied asymmetric air-gap, while Figure 8 displays the cogging torque waveforms and no-load phase voltage waveforms for both the symmetric and asymmetric air-gap models. In the cogging torque waveform of Figure 8, it is clear that applying an asymmetric air-gap creates a phase difference compared to a symmetric air-gap, generating regions with no zero-torque for both the cogging and magnetic torques. However, it is noteworthy that the application of an asymmetric air-gap causes a change in the phase of the phase voltage waveform, requiring adjustment of the current phase angle to 0 degrees.
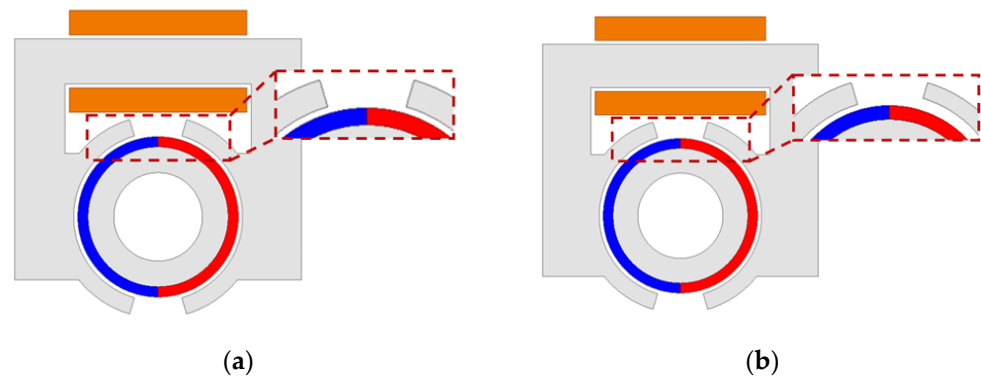
Figure 7. The shapes of the symmetric air-gap model and the model with applied asymmetric air-gap are as follows: (**a**) symmetric air-gap model; and (**b**) asymmetric air-gap model.
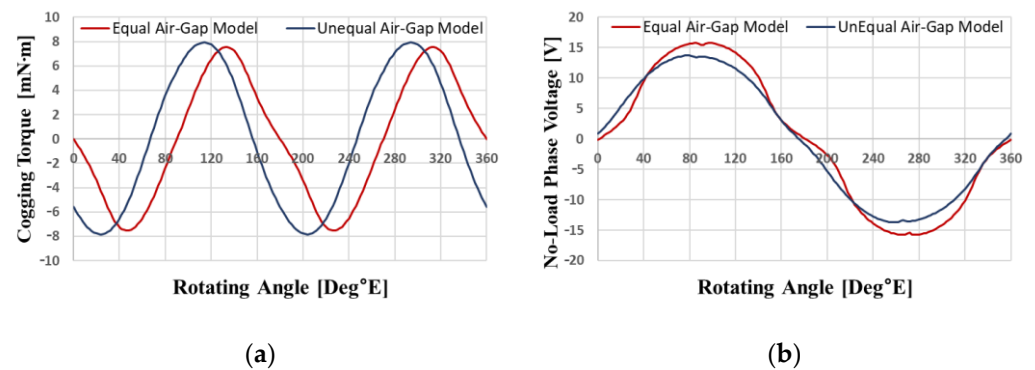

Figure 8. Comparison of cogging torque and no-load phase voltage waveforms between symmetric air-gap model and asymmetric air-gap model: (**a**) cogging torque waveform; and (**b**) no-load phase voltage waveform.

Table 1 presents the torque values for the symmetrical and asymmetrical air gap models. When comparing the load torque values of the two models, the symmetrical air gap structure has a torque of 25.8 mNm, whereas the asymmetrical air-gap structure has a torque of 23.2 mNm, signifying an approximate drop of 10% in torque value. Therefore, this paper aims to review the symmetrical air-gap structure when designing a single-phase BLDC motor, including a 10% margin in the load torque, before exploring the application of the asymmetrical air-gap structure.

Table 1. Torque comparison between the symmetrical and asymmetrical air-gap models.

Parameter	Symmetrical Air-Gap	Asymmetrical Air-Gap	Unit
Torque	25.8	23.2	mNm

3. Designing a Single-Phase BLDC Motor That Meets the Target Performance

3.1. Comparison of Single-Phase BLDC Motor Types

There are four types of single-phase BLDC motors applied in this study: C-Type, R-Type, internal rotor type, and external rotor type. C-Type and R-Type have angular shapes instead of the traditional cylindrical shape, which can reduce manufacturing costs by reducing scrap during production. In the C-Type configuration, the magnetic flux crosses each pole on a singular path, whereas in the R-Type configuration, the magnetic flux crosses each pole on a split path [21]. Due to C-Type's higher magnetic flux per pole compared to R-Type at the same output, less coil is required to achieve similar results, thereby reducing

costs. As a result, C-Type was chosen for the design to meet the performance target. Figure 9 illustrates the magnetic flux patterns for both C-Type and R-Type motors.
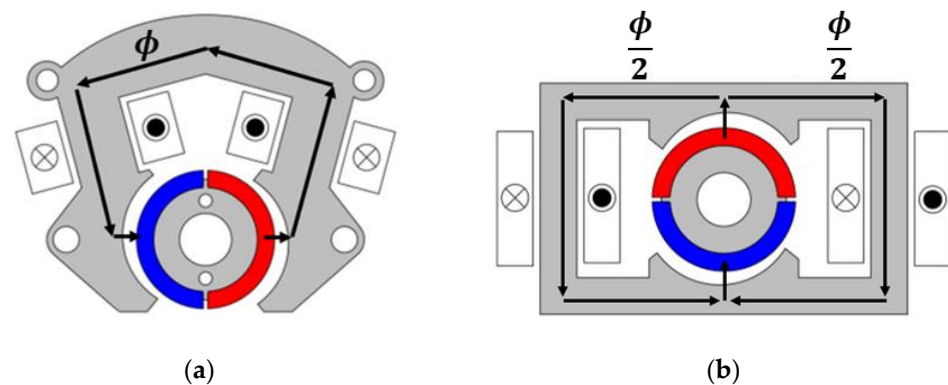

(**a**)　　　　　　　　　　　　　　　　　　　　(**b**)

Figure 9. Magnetic flux path comparison: (**a**) Magnetic flux path of C-Type BLDC motor; and (**b**) magnetic flux path of R-Type BLDC motor.

The internal rotor and external rotor types feature a cylindrical design, resulting in reduced stator core material usage. According to Equation (9), the external rotor design outperforms the internal rotor design in terms of performance. In Equation (9), *ac* represents the specific electric charge divided by the total electric charge from the void to the circumference, *k* represents the winding factor, and $\hat{B}_{g1}$ is a fundamental component of the magnetic flux density in air gap [22]. The design of a model that meets target performance parameters necessitated the selection of the external rotor type from among both internal and external rotor types. Figure 10 illustrates the variations in air-gap diameters observed between the two types.

$$T = \frac{\pi}{4}\left(k\hat{B}_{g1}ac\cos\beta\right)D^2{}_g L_{stk} \tag{9}$$

(**a**)　　　　　　　　　　　　　　　　　　　　(**b**)

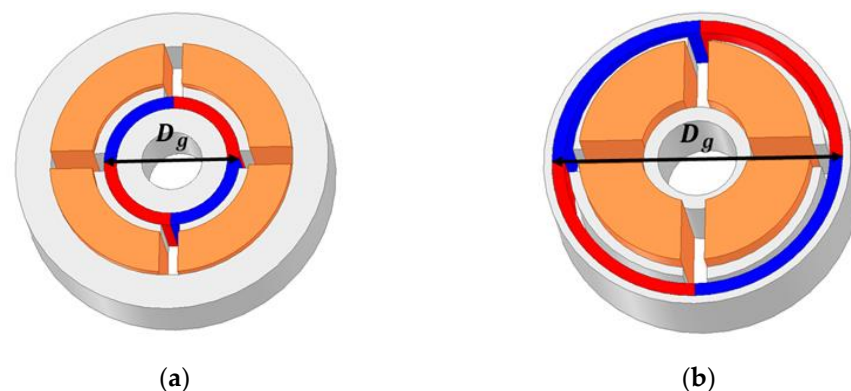**Figure 10.** Comparison of air-gap diameter: (**a**) internal rotor type BLDC motor air-gap diameter; and (**b**) external rotor type BLDC motor air-gap diameter.

3.2. Derivation of the Target Performance-Satisfying Model for an C-Type Single-Phase BLDC Motor

Table 2 presents the target performance and specifications of the C-Type single-phase BLDC motor. The symmetrical air-gap model will be used in this design, with consideration for a torque margin of 10% due to the asymmetric pole.

Table 2. C-Type single-phase BLDC motor target performance and specifications.

Parameter	C-Type Single Phase BLDC Motor	Unit
Poles	2	-
Slots	2	-
Rated Speed	2950	rpm
Rated Power	5	W
Rated Torque	15	mNm
Stack Length	11.2	mm
Fill Factor	50	%
Current Density	8	A_{rms}/mm^2
R_{on}	1.7	Ohm
Current Limit	1.5	A
Maximum Outer Size	61×60	mm
Core Material	35PN440	-
Permanent Magnet Material	HMG-12L (Nd-Bonded)	-
Coil Material	Copper	-

The single-phase C-type BLDC motor has a configuration comparable to the conventional SPIM. Accordingly, the initial design was carried out with the same dimensions as the induction motor represented in Figure 1. Figure 11 illustrates the configuration of the designed C-Type single-phase BLDC motor. The number of turns per phase required to meet the target torque was calculated. Table 3 presents the performance of the initial design model.

(**a**)	(**b**)
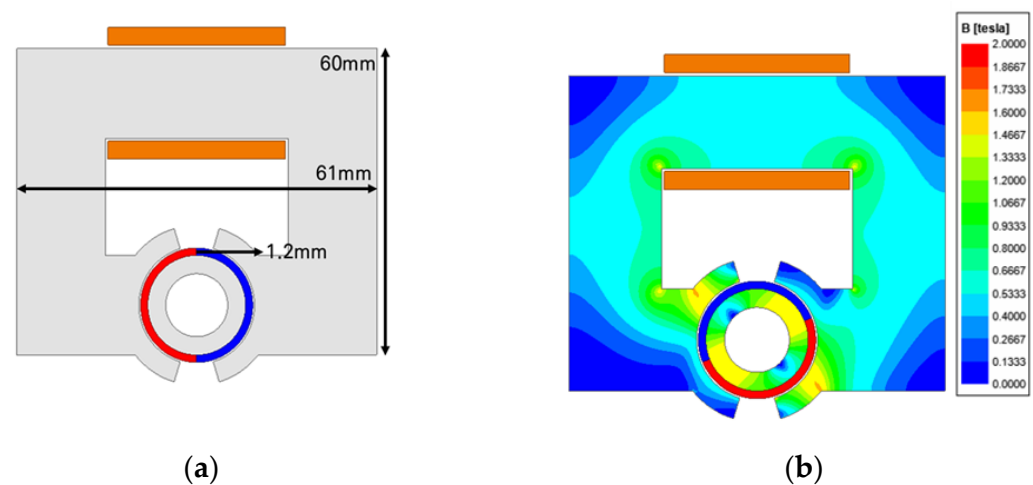
Figure 11. The initial design model of the C-Type single-phase BLDC motor: (**a**) configuration of initial design model; and (**b**) the initial design model's magnetic flux density at saturation.

Table 3. Performance of the basic design model of the C-Type single-phase BLDC motor.

Parameter	C-Type Basic Design Model	Unit
Power	6.3	W
Torque	19.3	mNm
Number of Turns	495	-
Current	0.486	A
Copper Loss	2.1	W
Iron Loss	0.164	W
Efficiency	75.5	%

In the case of the initial design model, performance exceeding the target was achieved, and the stator did not saturate. Therefore, a design was conducted to increase the magnetic loading and decrease the electrical loading. Additionally, a design was carried out to reduce

the stator size based on the saturation characteristics, resulting in a model that satisfies the target performance. The use of magnets in this target performance satisfying model increased (from a previous magnet thickness of 1.2 mm to 1.9 mm), while the amount of winding and core material usage decreased.

Furthermore, in order to improve the precision of the analysis, an analysis of Drive IC integration was performed. During this process, current limitations were established, taking margins into account. When integrating the Drive IC with the model designed to meet the desired performance criteria, it was observed that due to dead time, the current limitations were exceeded, and performance exceeding the desired goals was achieved. The voltage input method utilized in the analysis of Drive IC integration leads to a decrease in current and torque as the number of turns increases. Therefore, an examination was performed on the current and torque for varying numbers of turns, and the number of turns(184Turns) that met the current constraints and the desired torque was chosen for the ultimate design. Figure 12 represents the current and torque graphs for different numbers of turns, and Figure 13 represents the configuration and magnetic flux density at saturation of the final model that meets the target performance of the C-Type single-phase BLDC motor. Figure 14 represents the current and torque waveforms of the final model during the Drive IC integration analysis. Table 4 presents the performance of the final model of the C-Type single-phase BLDC motor.
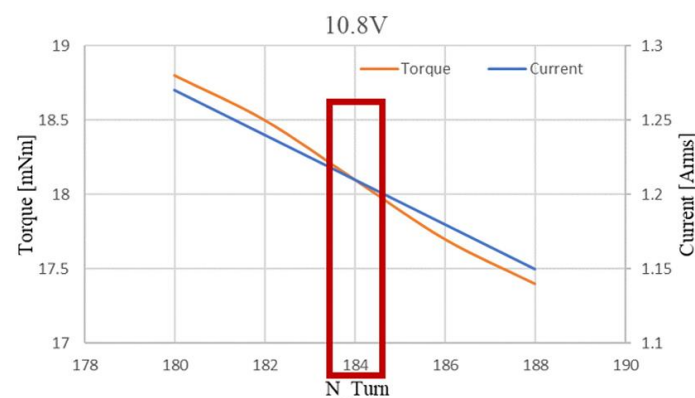

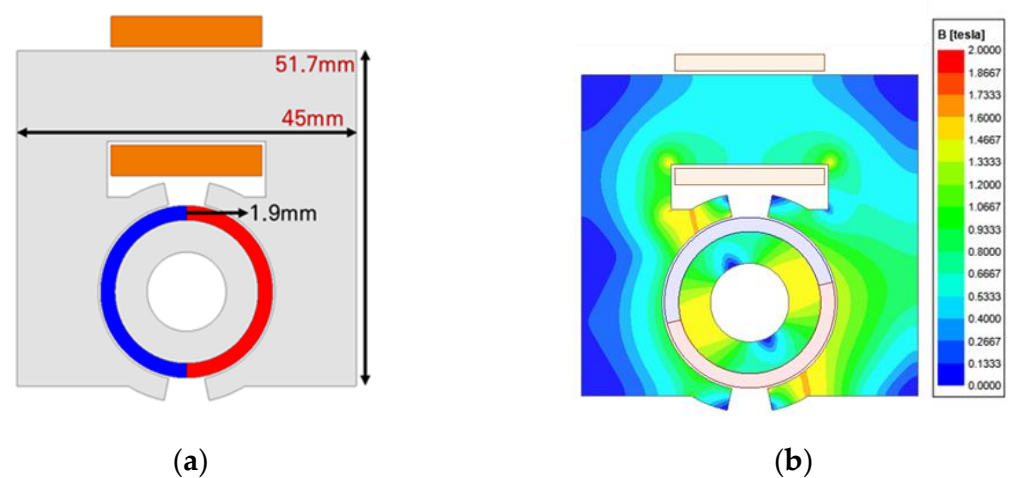**Figure 12.** Current and torque graphs for different numbers of turns.

(**a**) (**b**)

Figure 13. C-Type single-phase BLDC motor final model: (**a**) final model configuration; and (**b**) final model magnetic flux density at saturation.
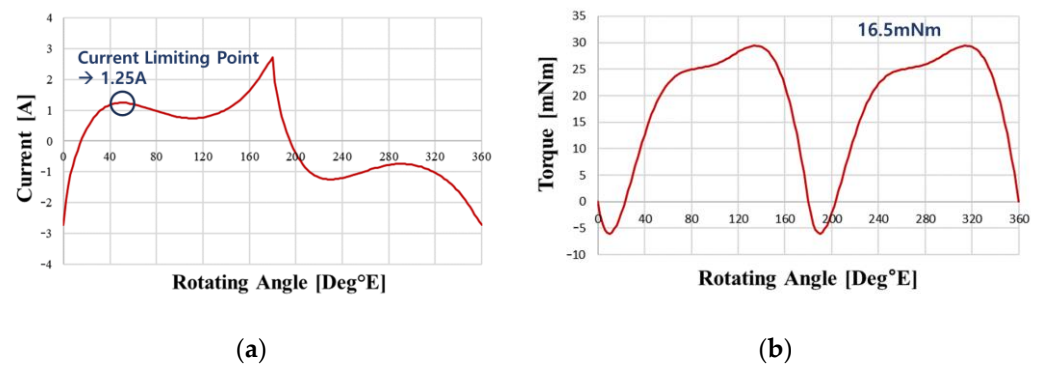
(**a**)

(**b**)

Figure 14. Waveforms during Drive IC integration analysis: (**a**) current waveform; and (**b**) torque waveform.

Table 4. Performance of the final model of the C-Type single-phase BLDC motor.

Parameter	C-Type Single Phase BLDC Motor	Unit
Power	5.1	W
Torque	16.5	mNm
Number of Turns	184	-
Current	1.25	A
Copper Loss	1.86	W
Iron Loss	0.31	W
Efficiency	68.3	%

3.3. Derivation of the Target Performance-Satisfying Model for an External Rotor Single-Phase BLDC Motor

Table 5 presents the target performance and specifications for the external rotor single-phase BLDC motor. In this design, the initially considered model is a symmetrical air-gap model, taking into account a torque margin of 10% due to asymmetric air-gap. Additionally, the limitations of the selected Drive IC were used to account for current limitations.

Table 5. External rotor type single-phase BLDC motor target performance and specifications.

Parameter	External Rotor Type Single Phase BLDC Motor	Unit
Poles	2	-
Slots	2	-
Rated Speed	2950	rpm
Rated Output	5	W
Rated Torque	15	mNm
Stack Length	11.2	mm
Fill Factor	50	%
Current Density	8	A_{rms}/mm^2
R_{on}	0.71	Ohm
Current Limit	1.8	A
Maximum Outer Diameter	39	mm
Core Material	35PN440	-
Permanent Magnet Material	HMG-4 (Nd-Bonded Magnet) HMG-12L (Nd-Bonded Magnet)	-
Coil Material	Copper	-

Figure 15 illustrates the relationship between torque and cost, as related to the increase in the number of turns and magnet usage. When the cost of increasing the number of turns and the magnet thickness is equal, it is more beneficial to increase the number of turns rather

than the magnet thickness for an increase in torque. The higher residual magnetic flux density of the HMG-12L Nd-bonded magnet saturates the core, which poses a challenge in achieving the necessary number of turns to attain the desired performance target. Therefore, a comparison of the saturation densities between Nd-Bonded Magnet HMG-4 and HMG-12L was conducted for the purpose of considering a change in magnet material. Table 6 indicates the residual magnetic flux densities of the examined magnets, and Figure 16 indicates the magnet saturation densities attained by applying Nd-Bonded Magnet HMG-4 and HMG-12L Designing with HMG-4 is preferable for securing the required number of turns, considering the magnet saturation density, compared to HMG-12L. Therefore, HMG-4 is utilized in the design.
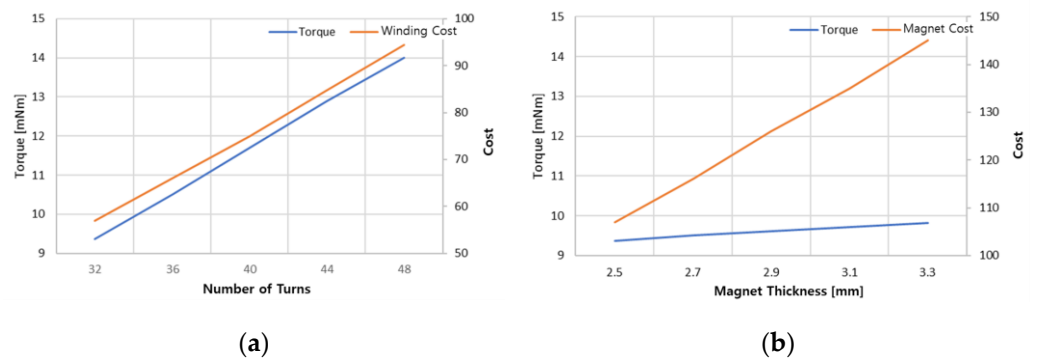

Figure 15. Torque and cost comparison graph: (**a**) with equal magnet usage and increasing turns; and (**b**) with equal turns and increasing magnet usage.

Table 6. Residual magnetic flux density by magnet material.

Material	Residual Magnetic Flux Density	Unit
HMG-4	0.47	
HMG-12L	0.75	T

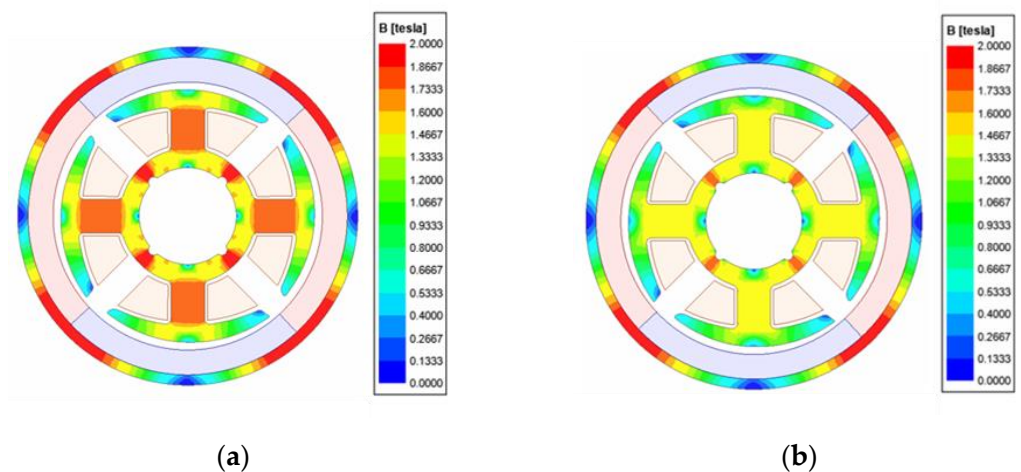**Figure 16.** Magnet saturation density when applying Nd-bonded magnet material: (**a**) HMG-12L; and (**b**) HMG-4.

The magnet material was replaced with HMG-4, and based on considerations of the stator core saturation characteristics and torque characteristics, a stator back yoke thickness of 1.65 mm was chosen. Figure 17 represents the torque characteristics with respect to the stator back yoke thickness. To meet the target performance, it was crucial

to secure the required number of turns. Therefore, the number of turns that satisfies the target performance was selected, considering the slot fill factor (50%) and current density (A_{rms}/mm^2 or below). Additionally, the motor outer diameter was determined accordingly.
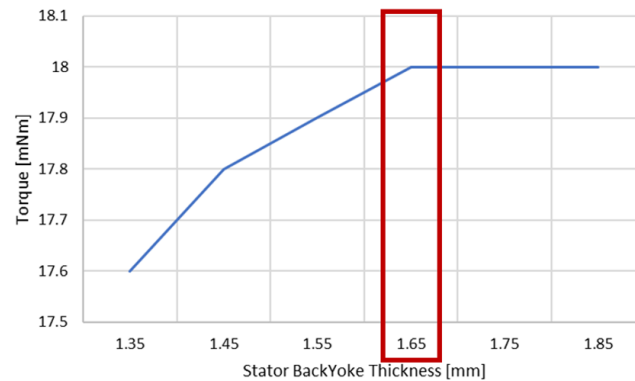

Figure 17. Torque characteristics graph with respect to stator back yoke thickness.

The target performance was achieved by selecting a total of 216 turns, taking into account the current limitation of the Drive IC, current density, and slot fill factor. To ensure the attainability of a viable phase angle for startup, an asymmetric air-gap was employed. The application of an asymmetric air-gap results in a shift in the phase of the cogging torque, allowing the magnetic torque to exceed zero at the point where the cogging torque reaches zero, enabling the motor to start. Due to the asymmetric air-gap structure, the voltage phase is changed. Therefore, the adjustment of the current phase angle to 0 degrees is necessary. Figure 18 represents the configuration of the model that meets the target performance, while Figure 19 represents the cogging torque and magnetic torque waveforms used to verify the feasibility of motor to start. Table 7 presents the performance of the target performance-satisfying model. It can be verified by Figure 19 that when the cogging torque reaches zero, the magnetic torque exceeds zero, demonstrating that the motor is capable of starting.
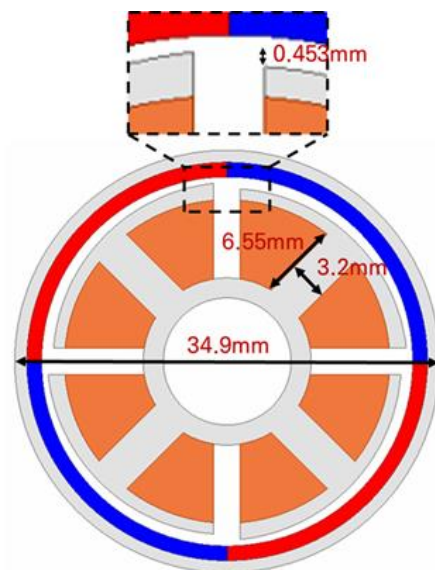

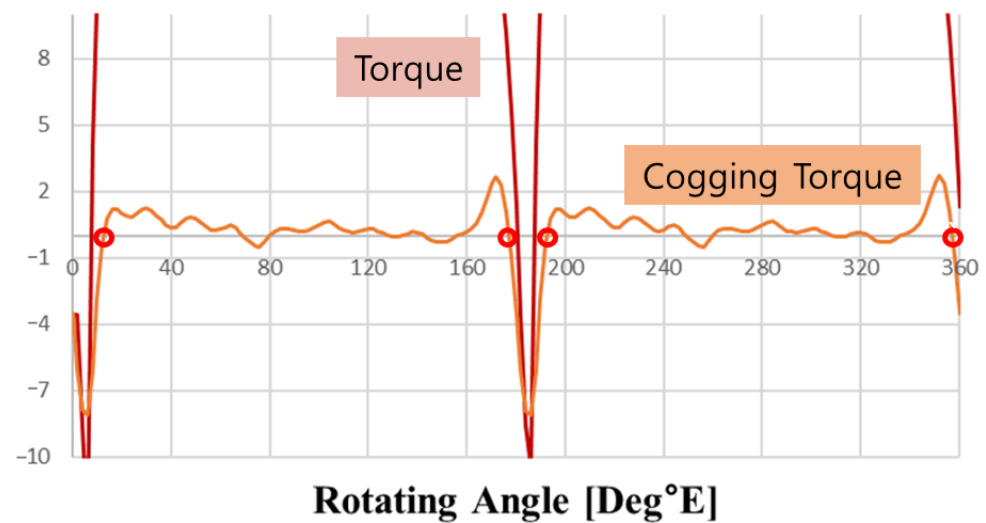**Figure 18.** Configuration of the model that meets the target performance.

Figure 19. Cogging torque and magnetic torque waveforms for verification the feasibility of motor to start.

Table 7. Performance of the target performance-satisfying model.

Parameter	External Rotor Type Single Phase BLDC Motor	Unit
Power	4.7	W
Torque	15.2	mNm
Number of Turns	216	-
Current	1.3	A
Copper Loss	1.67	W
Iron Loss	0.215	W
Efficiency	69.3	%

Having a low shoe thickness compared to the shoe length in the stator core may potentially result in manufacturing issues in small motors. Therefore, when designing the stator for a single-phase external rotor BLDC motor, it is advantageous to have a greater shoe thickness relative to the shoe length. In designing the final model for the external rotor single-phase BLDC motor that meets the target performance, the outer diameter was set at 34.9 mm. Taking into account the maximum outer diameter of the motor as per target specifications, which is 39 mm, the minimum possible thickness of the shoe was considered during the design process. The length of the slot opening was increased by 30.4% to reduce the length of the shoe. Additionally, the thickness of the shoe was increased by 21% to confirm its manufacturability. The magnet's thickness was determined based on the torque increase rate to achieve the desired performance. Figure 20 represents the torque increase rate with respect to magnet thickness. The required number of turns per phase was calculated to achieve the desired performance. The motor's outer diameter was determined by considering the slot fill factor and current density, while increasing shoe thickness. The design of the external rotor single-phase BLDC motor was finalized by integrating a Drive IC. Figure 21 represents the configuration and magnetic flux density at saturation of the final model with applied parameter changes and Figure 22 represents the current waveform when considering the Drive IC.
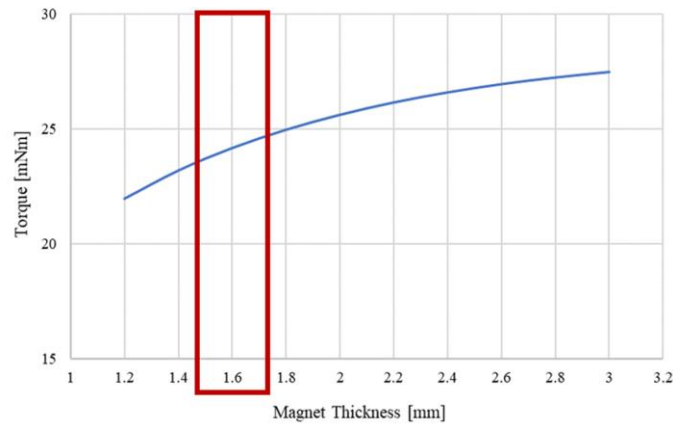
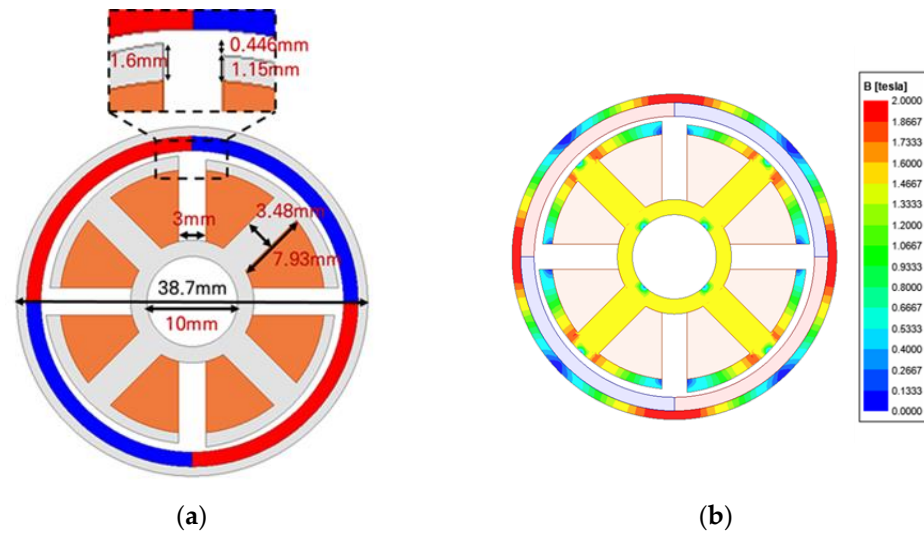**Figure 20.** Torque increase rate with respect to magnet thickness.

Figure 21. Outer rotor single-phase BLDC motor final model with applied parameter changes: (**a**) final model configuration; and (**b**) final model magnetic flux density at saturation.
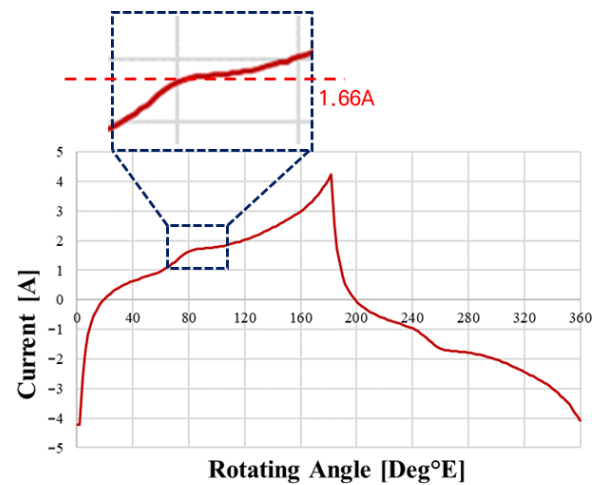

Figure 22. Current waveform when considering the Drive IC.

Incorporating the soft ON and OFF function results in reduced current, as seen in the current waveform in Figure 6. Therefore, further FEA analysis is necessary via additional current waveforms. During the assessment of the Drive IC integration, the input current

was estimated by analyzing the current waveform when implementing the soft ON and OFF features. It was confirmed through finite element analysis (FEA) that the desired performance is achieved when the input current is implemented as 1.66 A. Figure 23 represents the current waveform and torque waveform when applying the soft ON and OFF function, and Table 8 presents the performance of the final model of the external rotor single-phase BLDC motor. Figure 24 represents the operating point of the motor. The design points have been chosen based on the highest speed and torque values within this operational region.
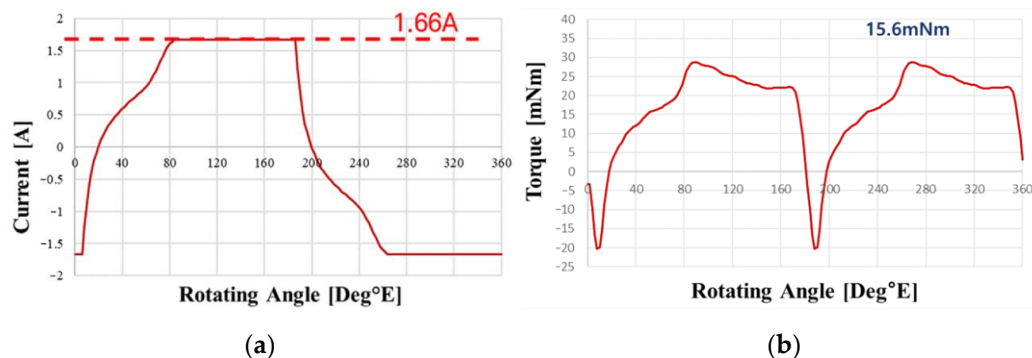

(a)   (b)

Figure 23. Expected current waveform and torque waveform when applying the soft ON and OFF function: (**a**) current waveform; and (**b**) torque waveform.

Table 8. Performance of the final model of the external rotor single-phase BLDC motor.

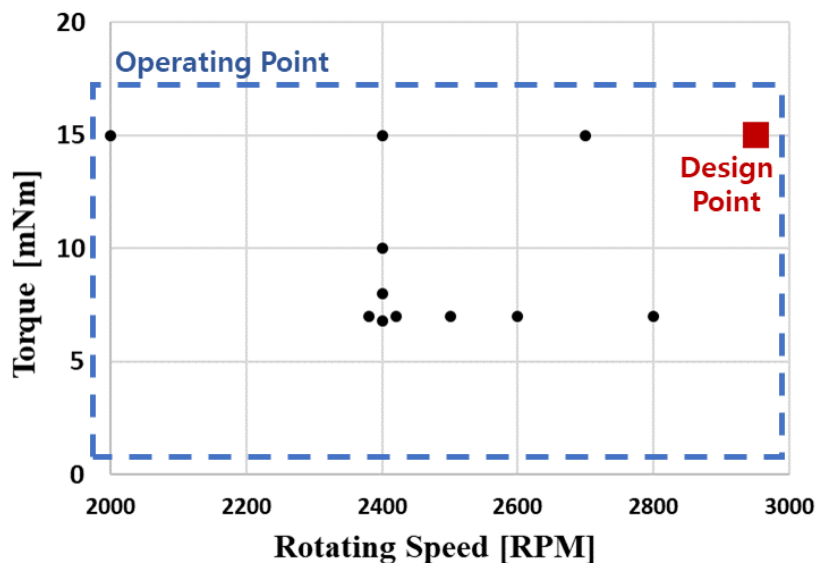| Parameter	External Rotor Single Phase BLDC Motor	Unit
Power	4.8	W
Torque	15.6	mNm
Number of Turns	228	-
Current	1.66	A
Copper Loss	2.51	W
Iron Loss	0.192	W
Efficiency	62.4	%

Figure 24. Operating point of the motor.

4. Selection of a Single-Phase BLDC Motor That Meets the Target Performance and Validation through the Production of a Prototype Motor

4.1. Selection of the Final Motor, Considering the Cost, for Both the C-Type and External Rotor Single-Phase BLDC Motors

Table 9 provides a comparison of the weights and costs of the final models of the C-Type and external rotor single-phase BLDC motors. The costs have been standardized based on the same year. For the C-Type motor, the magnetic flux density is higher due to the single flux path compared to the external rotor motor. Therefore, reduced copper usage is realized in the windings. However, due to the angular shape characteristics, the use of the stator core in the external rotor motor increases by approximately five times, ultimately leading to a higher final cost. Therefore, the oven fan motor requires low output and cost characteristics, and thus a single-phase BLDC motor was chosen as the optimal model.

Table 9. Comparison of the weights and costs between the C-Type and external rotor single-phase BLDC motors.

Parameter	C-Type Single Phase BLDC Motor	Outer Rotor Single Phase BLDC Motor	Unit
Stator Core (35PN440)	0.123	0.025	
Rotor Core (35PN440)	0.017	0.011	kg
Magnet(HMG-12L/HMG-4)	0.009	0.012	
Coil (Copper)	0.015	0.017	
Stator Core (35PN440)	209.4	42.1	
Rotor Core (35PN440)	29.3	18.5	
Magnet (HMG-12L/HMG-4)	57.6	59.4	KRW
Coil (Copper)	145.3	160.5	
Sum	441.6	280.4	

4.2. Prototype Motor Production and Validation

A prototype motor of the proposed external rotor single-phase BLDC motor was produced and tested to validate the feasibility of the Drive IC integration analysis. Soft ON and soft OFF functionality was utilized during the testing. To account for dead time, T_r and T_f were set to 10 μdeg. Figure 25 represents the prototype motor's configuration. Figure 26 represents the expected current waveform considering the soft ON and soft OFF function, while Figure 27 represents the current waveform obtained during the testing of the prototype motor. In Figure 27, the *x*-axis represents time, and the *y*-axis represents current. Table 10 presents the output and torque values obtained through FEA and those obtained through testing. This demonstrates the validity of the full-bridge inverter (Drive IC) integration analysis proposed in this paper.
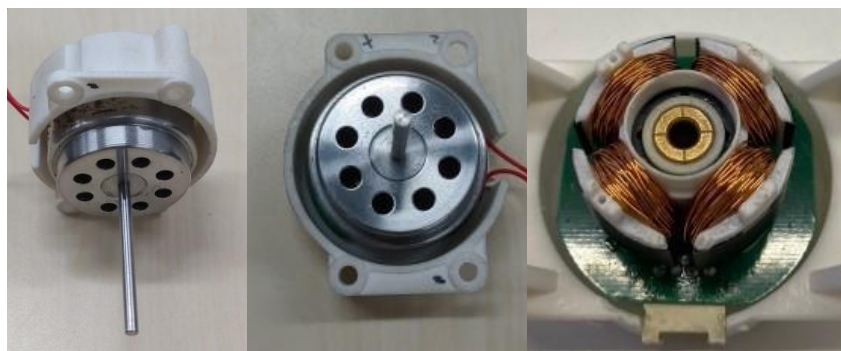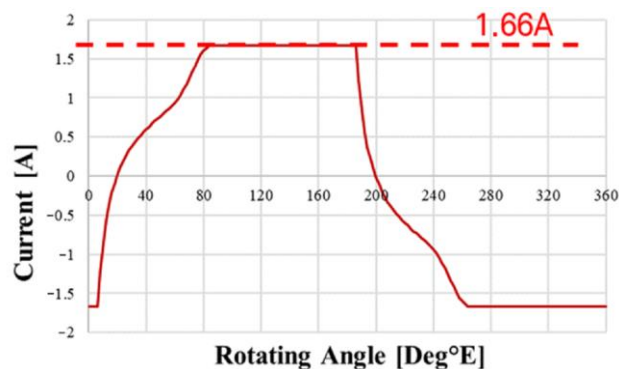
Figure 25. Prototype motor's configuration.

Figure 26. Expected current waveform considering the soft ON and soft OFF function.
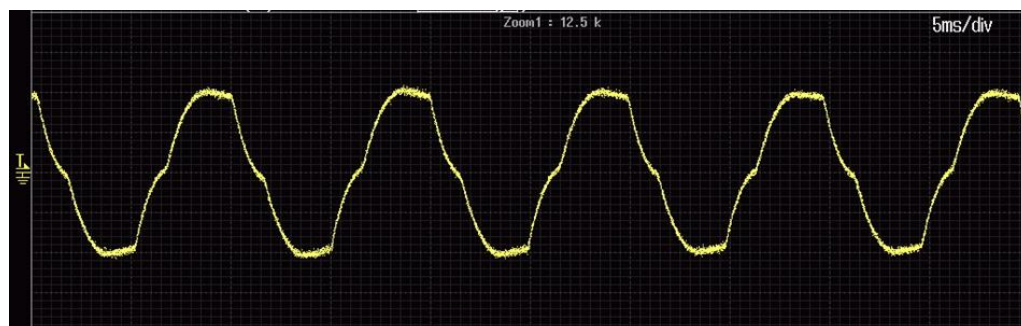

Figure 27. Current waveform obtained during the testing of the prototype motor.

Table 10. Comparison of the performance between the single-phase BLDC motor at 2950 rpm based on FEA and the prototype motor.

Parameter	FEA	Test	Unit
Power	4.8	4.7	W
Torque	15.6	15.0	mNm

5. Conclusions

This paper conducted a study on the design and analytical methods or a single-phase BLDC motor to replace SPIM. The study concentrated on an external rotor single-phase BLDC motor that meets the target performance and cost savings, enabling variable speed control. Furthermore, it is crucial to take into account the dead time of the full-bridge inverter (Drive IC) as single-phase BLDC motors mainly rely on this type of inverter. To address this concern, a Drive IC integration analysis method was proposed. The study compared various types of single-phase BLDC motors, designed models that met

performance targets, and analyzed the integration of the Drive IC. Additionally, a prototype motor was produced and verified through testing. The analysis of integrating the Drive IC through FEA and prototype motor testing revealed output discrepancies of about 2% and torque variances of approximately 4%. The test results indicate that the Drive IC integration analysis method conducted via FEA is valid.

Author Contributions: Conceptualization, W.-H.K. and D.-H.J.; methodology, Y.-S.L.; software, Y.-S.L.; validation, Y.-S.L.; formal analysis, N.-R.J.; investigation, H.-J.P.; resources, Y.-S.L.; data curation, N.-R.J.; writing—original draft preparation, Y.-S.L.; writing—review and editing, H.-J.P. and D.-H.J.; visualization, Y.-S.L. and D.-H.J.; supervision, W.-H.K. and D.-H.J.; project administration, W.-H.K. and D.-H.J. All authors have read and agreed to the published version of the manuscript.

Data Availability Statement: Not applicable.

Conflicts of Interest: The authors declare no conflict of interest.

References

1. Ojaghi, M.; Daliri, S. Analytic Model for Performance Study and Computer-Aided Design of Single-Phase Shaded-Pole Induction Motors. *IEEE Trans. Energy Convers.* **2016**, *32*, 649–657. [CrossRef]
2. Sharma, U.; Singh, B. Design and Development of Energy Efficient Single Phase Induction Motor For Ceiling Fan Using Taguchi's Orthogonal Arrays. *IEEE Trans. Ind. Appl.* **2021**, *57*, 3562–3572. [CrossRef]
3. Ahmed, F.; Kar, N.C. Analysis of End-Winding Thermal Effects in a Totally Enclosed Fan-Cooled Induction Motor With a Die Cast Copper Rotor. *IEEE Trans. Ind. Appl.* **2017**, *53*, 3098–3109. [CrossRef]
4. Cavagnino, A.; Lazzari, M.; Profumo, F.; Tenconi, A. A comparison between the axial flux and the radial flux structures for PM synchronous motors. *IEEE Trans. Ind. Appl.* **2002**, *38*, 1517–1524. [CrossRef]
5. Zhao, N.; Liu, W. Loss Calculation and Thermal Analysis of Surface-Mounted PM Motor and Interior PM Motor. *IEEE Trans. Magn.* **2015**, *51*, 8112604. [CrossRef]
6. Kim, T.-J.; Hwang, S.-M.; Kim, K.-T.; Jung, W.-B.; Kim, C.-U. Comparison of dynamic responses for IPM and SPM motors by considering mechanical and magnetic coupling. *IEEE Trans. Magn.* **2001**, *37*, 2818–2820. [CrossRef]
7. Dong, J.; Huang, Y.; Jin, L.; Lin, H. Comparative Study of Surface-Mounted and Interior Permanent-Magnet Motors for High-Speed Applications. *IEEE Trans. Appl. Supercond.* **2016**, *26*, 5200304. [CrossRef]
8. Zhao, W.; Yang, Z.; Liu, Y.; Wang, X. Analysis of a Novel Surface-Mounted Permanent Magnet Motor With Hybrid Magnets for Low Cost and Low Torque Pulsation. *IEEE Trans. Magn.* **2021**, *57*, 8104804. [CrossRef]
9. Pang, Y.; Zhu, Z.Q.; Feng, Z.J. Cogging Torque in Cost-Effective Surface-Mounted Permanent-Magnet Machines. *IEEE Trans. Magn.* **2011**, *47*, 2269–2276. [CrossRef]
10. He, T.; Zhu, Z.; Eastham, F.; Wang, Y.; Bin, H.; Wu, D.; Gong, L.; Chen, J. Permanent Magnet Machines for High-Speed Applications. *World Electr. Veh. J.* **2022**, *13*, 18. [CrossRef]
11. He, C.; Wu, T. Analysis and design of surface permanent magnet synchronous motor and generator. *CES Trans. Electr. Mach. Syst.* **2019**, *3*, 94–100. [CrossRef]
12. Chen, Y.-T.; Chiu, C.-L.; Jhang, Y.-R.; Tang, Z.-H.; Liang, R.-H. A Driver for the Single-Phase Brushless DC Fan Motor With Hybrid Winding Structure. *IEEE Trans. Ind. Electron.* **2012**, *60*, 4369–4375. [CrossRef]
13. Lee, W.; Kim, J.H.; Choi, W.; Sarlioglu, B. Torque Ripple Minimization Control Technique of High-Speed Single-Phase Brushless DC Motor for Electric Turbocharger. *IEEE Trans. Veh. Technol.* **2018**, *67*, 10357–10365. [CrossRef]
14. Dunkl, S.; Muetze, A.; Schoener, G. Design Constraints of Small Single-Phase Permanent Magnet Brushless DC Drives for Fan Applications. *IEEE Trans. Ind. Appl.* **2015**, *51*, 3178–3186. [CrossRef]
15. Fazil, M.; Rajagopal, K.R. Nonlinear Dynamic Modeling of a Single-Phase Permanent-Magnet Brushless DC Motor Using 2-D Static Finite-Element Results. *IEEE Trans. Magn.* **2011**, *47*, 781–786. [CrossRef]
16. Kim, S.-H. *Electric Motor Control DC, AC, and BLDC Motors*; Elsevier Science: Amsterdam, The Netherlands, 2017; pp. 275–335.
17. Yang, Y.; Zhou, K.; Wang, H.; Blaabjerg, F. Analysis and Mitigation of Dead-Time Harmonics in the Single-Phase Full-Bridge PWM Converter With Repetitive Controllers. *IEEE Trans. Ind. Appl.* **2018**, *54*, 5343–5354. [CrossRef]
18. Fazil, M.; Rajagopal, K.R. A Novel Air-Gap Profile of Single-Phase Permanent-Magnet Brushless DC Motor for Starting Torque Improvement and Cogging Torque Reduction. *IEEE Trans. Magn.* **2010**, *46*, 3928–3932. [CrossRef]
19. Park, Y.-U.; Cho, J.-H.; Kim, D.-K. Cogging Torque Reduction of Single-Phase Brushless DC Motor With a Tapered Air-Gap Using Optimizing Notch Size and Position. *IEEE Trans. Ind. Appl.* **2015**, *51*, 4455–4463. [CrossRef]

20. Kwon, B.-I.; Yang, B.-Y.; Park, S.-C.; Jin, Y.-S. Novel topology of unequal air gap in a single-phase brushless DC motor. *IEEE Trans. Magn.* **2001**, *37*, 3723–3726. [CrossRef]
21. Choo, Y.; Hwang, H.; Cho, J.; Kim, C.; Kim, J.; Hwang, S.-H.; Choi, J.Y.; Lee, C. Investigation of Systematic Efficiency in a High-Speed Single-Phase Brushless DC Motor Using Multi-Physics Analysis for a Vacuum Cleaner. *IEEE Trans. Magn.* **2019**, *55*, 8203606. [CrossRef]
22. Aydin, M.; Huang, S.; Lipo, T. Torque quality and comparison of internal and external rotor axial flux surface-magnet disc machines. *IEEE Trans. Ind. Electron.* **2006**, *53*, 822–830. [CrossRef]